Proceedings of the ASME 2010 3rd Joint US-European Fluids Engineering Summer Meeting and 8th International Conference on Nanochannels, Microchannels, and Minichannels
FEDSM-ICNMM2010
August 1-5, 2010, Montreal, Canada

FEDSM-ICNMM2010-30303

EXPERIMENTAL AND THEORETICAL STUDIES OF PULSED MICRO FLOWS PERTINENT TO CONTINUOUS SUBCUTANEOUS INSULIN INFUSION (CSII) THERAPY

Wang, Bin and Hu, Hui (✉)
Department of Aerospace Engineering
Iowa State University, Ames, IA 50011
Email: huhui@iastate.edu

Demuren, Ayodeji
Department of Mechanical Engineering
Old Dominion University, Norfolk, VA 23529

and

Gyurcsko, Eric
Children's Hospital of The King's Daughters,
Eastern Virginia Medical School, Norfolk, VA 23501

ABSTRACT

Continuous subcutaneous insulin infusion (CSII) therapy, also known as insulin pump therapy, has become an important advancement in diabetes therapy to improve the quality of life for millions of diabetes patients. Insulin delivery failures caused by the precipitations of insulin within micro-sized CSII tubing systems have been reported in recent years. It has also been conjectured that the flow of insulin through an insulin infusion set may be reduced or inhibited by air bubbles entrained into the capillary CSII tubing system during the typical three- to five-day operation between refills. Currently, most solutions to insulin occlusion related problems are based on clinical trials. In the present study, an experimental and theoretic study was conducted to investigate the pulsed flows inside the micro-sized CSII tubing system. A micro-PIV system was used to provide detailed flow velocity field measurements inside the capillary CSII tubing system to characterize the transient behavior of the micro-flows upon the pulsed actuation of the insulin pump used in CSII therapy. It was found that the microflow inside the CSII tubing system is highly unsteady, which is much more interesting than the creeping flow that the nominal averaged flow rates would suggest. A theoretic frame work was also performed to model the pulsed micro-flows driven by the insulin pump to predict the transient behavior of the microflows and velocity distributions inside the micro-sized CSII tubing system. The measurement results and the theoretic predictions were compared quantitatively to elucidate underlying physics for a better understanding of the microphysical process associated with the insulin delivery in order to provide a better guidance for troubleshooting of insulin occlusion in CSII therapy.

INTRODUCTION

In recent years, there has been a surge in the use of continuous subcutaneous insulin infusion (CSII), also known as insulin pump therapy, as opposed to the more traditional use of multiple daily injection (MDI) therapy to treat Type 1 diabetes (Alemzadeh, 2004; Shalitin and Philips, 2008). CSII delivers insulin to the person with diabetes continuously, simulating the natural internal secretion of insulin from the pancreas (Rossetti et al. 2008). Major advantages of CSII over MDI include: more precise amounts of insulin can be delivered as needed than by use of a syringe; better control over background or 'basal' insulin dosage can be gained to meet all the body's non-food related insulin needs; insulin pump software automatically determines the 'bolus' infusion dosages based on expected carbohydrate intake and current blood sugar level (Bruttomesso, 2009).

During CSII, insulin must travel from the insulin pump's reservoir, through various lengths of micron-sized capillary tubing, infusion set, and finally via a catheter to the patient's subcutaneous space, without occlusion. This must occur accurately, regardless of ambient temperature, the activity level of the patient, or low basal infusion rates. Young children require very small amounts of insulin to manage their diabetes. This results in a very slow rate of continuous insulin infusion, often on the order of 1.0 μL (or 0.1 units of insulin) per hour.

As a consequence of this slow infusion rate, occlusion to insulin flow can, and often does, occur. There is anecdotal evidence, supported by results of comprehensive surveys (Hartman, 2008; Weissberg-Benchell, 2007), that the actual insulin delivery dosage might fall short of the pre-programmed value at relatively low flowrates, leading to reduced glycemic control. Occlusion of insulin delivery, if not detected and immediately treated, may result in severe, sustained hyperglycemia or diabetic ketoacidosis (DKA). Frequent occlusive episodes may result in sub-optimal glycemic control, elevated hemoglobin A1C values, and an increased risk of long-term complications of diabetes (Weissberg-Benchell, 2007). Case studies presented by Poulsen et al. (2005) and Wolpert et al. (2002) suggest that delivery failure may be caused by precipitation of insulin within the infusion set. There are also speculations that the flow of insulin through the infusion set may be reduced or impaired by air bubbles entrained in the micron-sized tubing system of the infusion set, during the typical 3 ~ 5 day operation between refills. To date, this is still a subject of much debate.

Currently, most solutions to insulin occlusion related problems are based on clinical trials. It is of great value to elucidate underlying physics of insulin infusion process, from the pump action to the catheter delivery, and from a fluid dynamics perspective, in order to provide a better guidance for troubleshooting. In this regard, Demuren & Doane (2007) and Demuren et al. (2009) carried out pioneer studies on the accuracy of insulin delivery by different pump types (Paradigm 511/512/712, Animas, and Omnipod) over a wide range of flow rates from 0.1 to 2.0 units per hour (U/H). They found that the operation of the insulin pumps was anything but continuous. The insulin pumps use stepper motors which operate for only a short moment each time. The screw pumps to which they are attached deliver 0.1 unit (i.e., 1.0 μL) each time. The consequence is that for an infant with a prescribed basal dosage of 0.1 U/H, an insulin pump only operates once per hour. If the flow was occluded in any way, it would have to wait another hour for the next delivery opportunity. On the other hand, an adult, with a typical basal dosage of 1.0 U/H, only have to wait for 6 minutes for the next delivery opportunity. Thus, dangers from occlusive events are much more severe in infants and young children than in adults. They also found that the unsteady flow features are the same for any insulin pumping pulses irrespective of nominal basal dosage; they merely occur more frequently at higher programmed dosages. Demuren et al. (2009) also observed air bubble formation in the reservoir and injection in infusion sets during experiments, but were unable to characterize the extent and overall impact of air bubbles on insulin delivery in CSII therapy.

It should be noted that the work of Demuren & Doane (2007) and Demuren et al. (2009) were based on bulk flow rate measurements, it is quite difficult, if not impossible, to extract detailed information (i.e., temporal-and-spatially-resolved flow field measurement results) to quantify the transient behavior of the unsteady micro-flows inside CSII tubing system from the bulk flow rate measurements. In the present study, a microscopic Particle Image Velocimetry (micro-PIV) system is used to conduct detailed flow velocity field measurements to characterize the transient behavior of the unsteady micro-flows inside a typical micro-sized CSII tubing system. The effects of the air bubbles entrained into the micro-sized tubing system on the insulin delivery process are also assessed based the detailed micro-PIV measurements. The objective of the study is to elucidate underlying physics for a better understanding of the microphysical process associated with the insulin delivery in order to provide a better guidance for the troubleshooting of insulin occlusion in CSII therapy.

EXPERIMENTAL SETUP AND MICRO-PIV MEASUREMENTS

Figure 1 shows the schematic of the experimental setup used in the present study. A Medtronic MiniMed Paradigm 512 insulin pump was used to drive the flow passing through a standard Paradigm Quick-Set infusion set. The inner diameter (I.D.) of the infusion tubing of the Paradigm Quick-Set infusion set is 350μm. The insulin pump uses a program-controlled proprietary stepper motor turning a captive lead screw that pushes the plunger on the reservoir, and delivers insulin in discrete 0.1 unit increments (1.0μL) per pulse cycle. In the present study, the insulin pump was set to operate in basal mode with the flow rate of 2.0 U/H (i.e., 20 μL per hour).

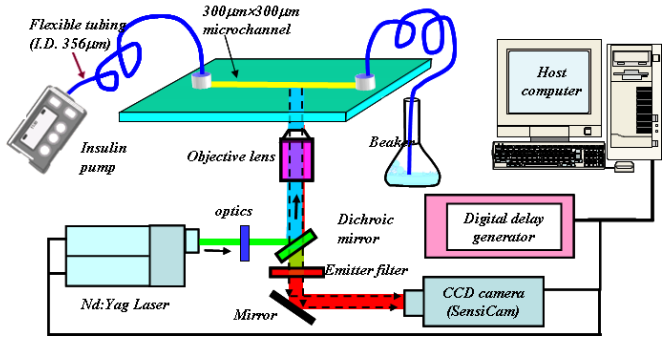

Fig. 1: Experimental setup

A micro-PIV system was used in the present study to conduct detailed flow velocity field measurements to characterize the transient behavior of the unsteady micro-flows driven by the insulin pump. The micro-PIV technique, which is the most commonly used tool for in-situ imaging of micro-flows, derives flow velocity vectors by observing the motions of tracer particles seeded in the flows (Santiago et al 1998; Meinhart et al. 1999; Olsen & Bourdon 2003, Kinoshita et al. 2007). It should be noted that, while microchannel flows driven by either pressure force (Santiago et al. 1998, Li & Olsen 2006), capillary effects (Prins et al. 2001, Gallardo et al. 1999), electric fields (Kim et al., 2002) or centrifugal forces (Johnson et al. 2001) have been studied extensively in recent years, majority of those previous studies were conducted with the micro-flows in steady state and driven by steady (time-invariant) compelling forces. In the present study, the micro-flow inside the micro-sized CSII tubing system was driven by a pulsed insulin pump, which have not been fully explored before.

Since the micro-sized tygon tubing of the standard Paradigm Quick-Set infusion set is only semi-transparent, as

shown in Fig. 1, a 38mm-long transparent microchannel (Translume Corp.) with cross section of 300×300μm (i.e., W = H =300μm) was used to act as a part of the CSII tubing system for the micro-PIV measurements. For simplicity, purified DI water, instead of insulin, was used as the working fluid in the present study. Nile red fluorescent FluoSpheres® beads (535/575nm, ~ 1μm in diameter) were premixed in the reservoir as the tracers for micro-PIV measurements. Illumination was provided by a double-pulsed Nd:YAG laser (NewWave) adjusted on the second harmonic and emitting two pulses of ~2 mJ per pulse at the wavelength of 532 nm. The repetition rate of the double-pulsed laser illumination was 10 Hz. Upon the pulsed excitations of the green laser beam at 532nm, the tracer particles seeded in the micro-flows will emit fluorescent light with an emission peak at 575nm. The fluorescence from the exited trace particles, which passes through a 10X objective lens (NA=0.4, depth of field about 5.0 μm), a long pass optic filter (580nm long pass filter) and the optical path inside an inverted microscope (Leica DM-IL), was recorded by a 12-bit high resolution (1376 x 1040 pixel) CCD camera (SensiCam-QE, Cooke Corp.). The CCD camera and the double-pulsed Nd:YAG laser were connected to a workstation (host computer) via a Digital Delay Generator (Berkeley Nucleonics, Model 565), which controlled the timing of the laser illumination and image acquisition. In the present study, the scaling factor of the acquired micro-PIV images was found to be 0.97μm/pixel. After micro-PIV images were acquired, instantaneous PIV velocity vectors were obtained by a frame to frame cross-correlation technique involving successive frames of patterns of particle images in an interrogation window 32×32 pixels. An effective overlap of 50% of the interrogation windows was employed in PIV image processing. The measurement uncertainty level for the measurements of the instantaneous velocity vectors was estimated to be within 2.0%.

RESULTS AND DISCUSSIONS

A. CHARACTERISTICS OF THE UNSTEADY MICRO-FLOW DRIVEN BY AN INSULIN PUMP

Fig. 2 shows typical micro-PIV measurement results at four time instants when the focal plane of the microscopic objective (depth of field ~5.0 μm) was set to the mid-plane of the 300 μm deep microchannel. The transient behavior of the unsteady micro-flow driven by the insulin pump was visualized clearly and quantitatively from the instantaneous flow velocity distributions. Based on the time sequences of the micro-PIV measurements, the histogram of the flow velocity at the center of the microchannel (i.e., streamwise-averaged centerline flow velocity) could be derived, which is given in Fig. 3. It can be seen clearly and quantitatively that the micro-flow inside the CSII tubing system was highly unsteady with the flow velocity changing significantly as a function of time. As expected, the period of the operation cycle of the insulin pump was found to be 180s when the insulin pump was set at 2.0 U/H basal rate. During each insulin pump operation cycle, the centerline flow velocity was found to be very small for most of the time, except within the short time period when the insulin pump operated. The time-averaged centerline velocity over each insulin pump operation cycle was also plotted in the figure as the red dash line for comparison. It can be seen clearly that the behavior of the micro-flow inside the CSII tubing system is much more interesting than a creeping flow that the nominal time-averaged flow velocity would suggest. While the time-averaged centerline velocity was only about 0.098 mm/s (i.e., corresponding a creeping flow at the Reynolds number Re_D = 0.030), the maximum centerline flow velocity inside microchannel at the end of the insulin pump operation pulse was found to be as high as 26.4 mm/s, which is more than 260 times higher than the time-averaged centerline flow velocity.

The dynamic response of the micro-flow inside the CSII tubing system upon the pulsed actuation of the insulin pump can be seen more clearly from the enlarged view of the centerline flow velocity variations before and after the operation pulse of the insulin pump, which is given in Fig. 4. It can be seen clearly that, while the period of the insulin pump operation cycle was 180s at the basal rate of 2.0 U/H, the real action time for the insulin pump was found to be only about 0.40s. The action time of 0.40s for the insulin pump estimated by the micro-PIV measurements was found to agree well with the value reported by Demuren et al. (2009). As shown in Fig. 4, the flow velocity inside the microchannel was found to be very small, i.e., almost zero, before the operation pulse of the insulin pump. A significant pressure head would be generated due to the pulsed actuation of the insulin pump. The flow velocity inside the infusion tubing system was found to increase rapidly as the insulin pump started to act. The centerline flow velocity was found to reach as high as 26.4 mm/s at the end of the insulin pump operation pulse. After the pulsed operation ended, no additional pressure head would be generated to drive the microflow. As a result, the microflow inside the CSII tubing system was found to begin to decelerate and experience a flow decay process. As shown clearly in Fig. 4, the decay process of the centerline flow velocity inside the microchannel was found to be fitted reasonably well by an exponential function with the characteristic decay time, τ = 0.16s.

Fig. 5 shows the normalized streamwise-averaged flow velocity profiles across the square microchannel at different time instants in the flow decay process after the pulsed action of the insulin pump. The time instant of $t=t_0$ corresponds to the end of the operation pulse of the insulin pump. Surprisingly, although the magnitude of the flow velocity inside the microchannel was found to decrease rapidly in the flow decay process, the normalized flow velocity data (i.e., normalized by the maximum flow velocity at the centerline of the microchannel) at different time instants was found to align nicely in the plots. It indicates that the flow velocity profiles across the microchannel were self-similar during the flow decay process.

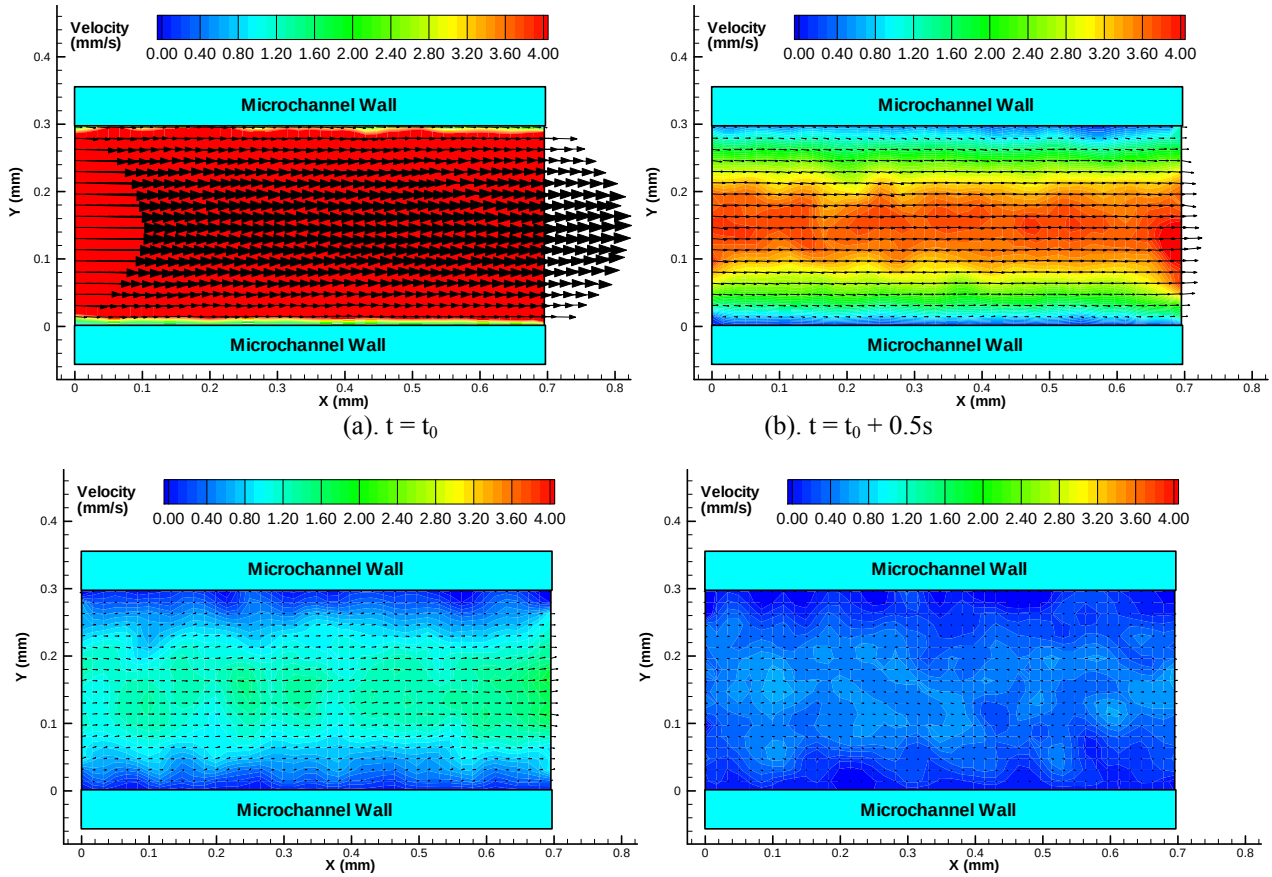

(a). $t = t_0$ (b). $t = t_0 + 0.5s$

(c). $t = t_0 + 1.0$ s (d). $t = t_0 + 5.0$ s

Fig. 2 : Instantaneous velocity distributions inside the microchannel at 2.0 U/H basal rate.

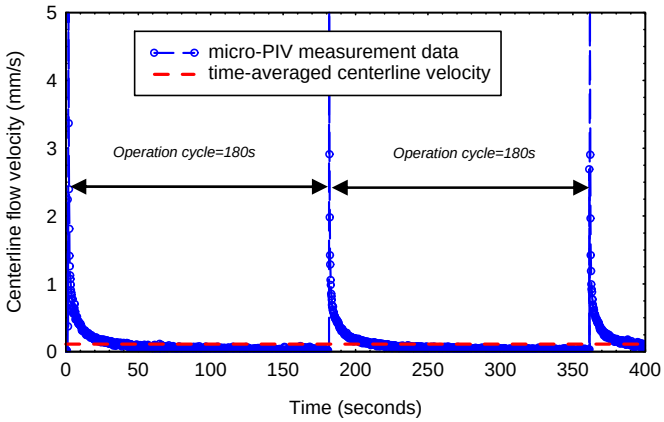

Fig. 3: Histogram of the centerline flow velocity at 2.0 U/H basal rate.

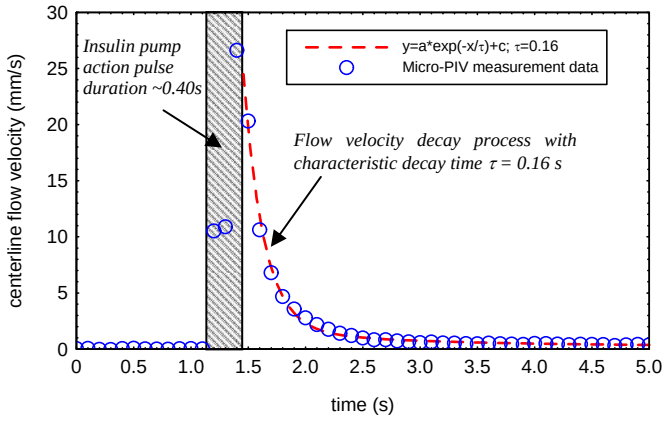

Fig. 4: Centerline flow velocity before and after an insulin pump action pulse

According to White (1991), for a fully-developed, pressure-driven laminar flow inside a rectangular channel of $-W/2 \le y \le W/2$ and $-H/2 \le z \le H/2$, the theoretical solution of the velocity distribution inside the rectangular channel can be expressed as:

$$U(y,z) = \frac{16h^2}{\mu\pi^3}\left(-\frac{dp}{dx}\right)\sum_{n=1,3,5,\ldots}^{\infty}(-1)^{(n-1)/2}\left[1-\frac{\cosh(n\pi z/H)}{\cosh(n\pi h/H)}\right]\frac{\cosh(n\pi y/W)}{n^3} \quad (1)$$

where W and H are the width and height of the rectangular channel, respectively. The term of $-dp/dx$ is the corresponding pressure gradient.

The theoretical solution given in Equation (1) for a fully-developed laminar channel flow as well as a parabolic curve fitting was also plotted in Fig. 5 for comparison. Interestingly, the measured velocity profiles across the microchannel were found to agree reasonably well with the theoretical solution for a fully-developed laminar channel flow even though the microflow was still in transient state during the flow decay process.

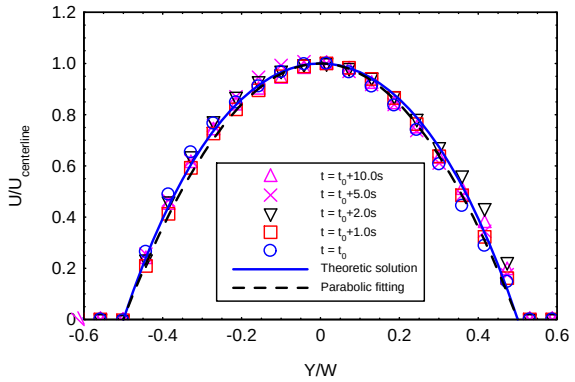

Fig. 5: Normalized flow velocity profiles at different time instants in the decay process.

In the present study, the micro-PIV measurements were also conducted at different depths of the square microchannel by adjusting the focal plane of the microscopic objective (depth of field ~ 5.0 μm) along the depth direction of the square microchannel. Fig. 6 shows the streamwise-averaged flow velocity profiles across the microchannel at different channel depths. The data shown in Fig. 6 was based on the same data reduction procedure as those shown in Fig. 5, but normalized by the local maximum flow velocity at each channel depth. The theoretical solution for a fully-developed laminar channel flow as expressed by Equation (1) and a parabolic curve fitting were also plotted in the figure for comparison. It can be seen clearly that the normalized flow velocity distributions at different channel depths can also be represented reasonably well by the theoretical solution. In summary, the micro-PIV measurements suggest that the theoretical solution for a fully-developed laminar channel flow expressed in Equation (1) can be used to estimate the flow velocity distribution inside the square microchannel even though the microflow was in transient state during the flow decay process.

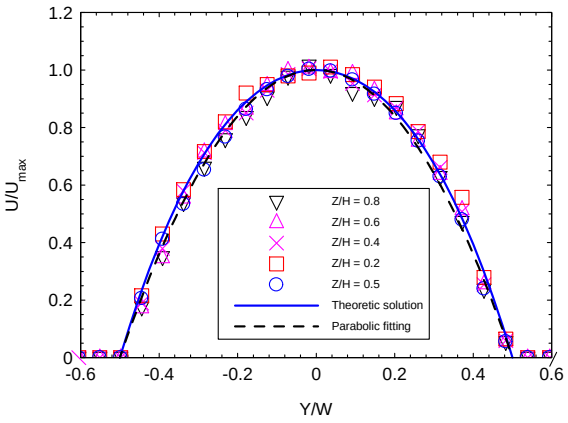

Fig. 6: Normalized velocity profiles at different channel depth.

B. THEORETICAL MODELING OF THE UNSTEADY MICRO-FLOW DRIVEN BY AN INSULIN PUMP

While several analytical studies have been conducted in recent years to investigate laminar, fully developed, pulsating and oscillating flows through microchannels for the purpose of cleaning enhancement (Ray et al. 2004, Celnik et al. 2006, Qi et al. 2008), no previous work can be found in literature to theoretically model transient behavior of the unsteady microflow inside the CSII tubing system upon the pulsed excitation of an insulin pump. In this section, a theoretical solution of the unsteady laminar flow inside the rectangular microchannel upon the pulsed excitation of an insulin pump will be derived. The theoretical predictions will be compared with the PIV measurement results quantitatively to elucidate underlying physics to improve our standing of the insulin delivery process in CSII therapy.

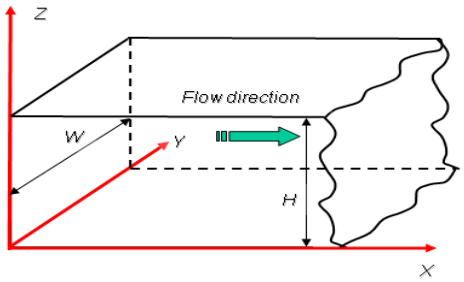

Fig. 7: Schematic of a flow through a rectangular channel

As shown in Fig. 7, we consider a fully developed laminar flow through a rectangular microchannel. The origin of the Cartesian coordinate system is located at one corner of the microchannel, with the flow in the x-axis direction. Based on the experimental results presented above, it is reasonable to make following assumptions for the flow inside the microchannel:

- Incompressible and Newtonian fluid with constant physical properties.
- Gravity effects are negligible.
- Pressure gradient is non-zero only along flow direction (i.e., X-direction).

- Flow velocities in the *Y* and *Z* directions are zero (i.e., Uni-directional flow).

Thus, Continuity equation and Navier-Stokes equations can be simplified as follows: (Leal 1992).

$$\frac{\partial u}{\partial x} = 0 \quad \Rightarrow \quad u = u(y,z,t) \tag{2}$$

$$\frac{\partial u}{\partial t} = -\frac{1}{\rho}\frac{\partial P}{\partial x} + \nu\left(\frac{\partial^2 u}{\partial y^2} + \frac{\partial^2 u}{\partial z^2}\right) \tag{3}$$

which subjects to no-slip boundary conditions at the wall $u(t,y,z) = 0$ for *y=0, y=W, z=0, z=H;* and stationary initial conditions $u(y,z,0) = 0$.

In the equations, *u* is the fluid velocity in the *x* direction. *y* and *z* are the directions normal to the flow direction. *W* is the width of the micro-channel; *H* is the height of the micro-channel. ρ is the density of the fluid, which is a constant in the present study. ν is the kinetic viscosity and $\partial P/\partial x$ is the pressure gradient.

Since velocity *u* is not the function of *x* as suggested by the continuity equation, $\partial P/\partial x$ must only be a function of time, *t*, for the uni-directional flow. Therefore, the equation (3) can be rewritten as

$$\frac{\partial u}{\partial t} = -f(t) + \nu\left(\frac{\partial^2 u}{\partial y^2} + \frac{\partial^2 u}{\partial z^2}\right) \tag{4}$$

where $f(t) = \frac{1}{\rho}\frac{\partial P}{\partial x}$. (5)

According to Fan and Chao (1965), Green function method can be used to deduce the solution of the flow velocity distribution inside a rectangular channel from the above governing equations, which can be expressed as follows:

$$G_u(y,z,t) = \frac{16}{\rho\pi^2}\sum_{n=0}^{\infty}\sum_{m=0}^{\infty}\frac{e^{-\nu\lambda^2_{mn}t}S_{2m+1,2n+1}}{(2m+1)(2n+1)} \tag{6}$$

where

$$\lambda^2_{nm} = \pi^2\left[\frac{(2m+1)^2}{W^2} + \frac{(2n+1)^2}{H^2}\right] \tag{7}$$

$$S_{2m+1,2n+1} = \sin\frac{(2m+1)\pi y}{W}\sin\frac{(2n+1)\pi z}{H} \tag{8}$$

Following the work of Qi *et al.* (2008), the transient response of the flow velocity inside a rectangular channel with arbitrary pressure gradients can be expressed as the convolution of pressure gradient and the Green's function as below:

$$u(y,z,t) = \int_0^t f(\tau)G_u(y,z,t-\tau)d\tau \tag{9}$$

where *f(t)* describes the arbitrary pressure gradient.

In the present study, the variations of the pressure inside the CSII tubing system upon the pulsed excitation of the insulin pump were measured by using digital pressure transducers. The transient pressure gradient inside the CSII tubing system can be determined based on the pressure measurement results, which was given in Fig. 8. The pulsed operation features of the insulin pump were revealed quantitatively from the time histogram of the measured pressure gradient inside the CSII tubing system. It can be seen clearly that the period of the pulsed operation cycle was 180s when the insulin pump was set at 2.0 U/H basal rate, which agrees well with the micro-PIV measurements shown in Fig. 3. The enlarged view of the pressure gradient variation in the vicinity of the operation pulse of the insulin pump was also given in the figure in order to elucidate the details of the dynamic changes of the pressure gradient inside the CSII tubing system before and after the operation pulse of the insulin pump. It can be seen clearly that, upon the actuation of the pulsed operation of the insulin pump, the pressure gradient inside the CSII tubing system would increase rapidly and to reach its peak value at the end of operation pulse. Based on the time-sequence of the pressure measurements at the data acquisition rate of 200Hz, the duration of the pump operation pulse was found to be about 0.40s, which agree with the value estimated based on the micro-PIV measurements. The pressure gradient inside the CSII tubing system was found to decrease rapidly after the pulsed operation of the insulin pump until next operation pulse starts.

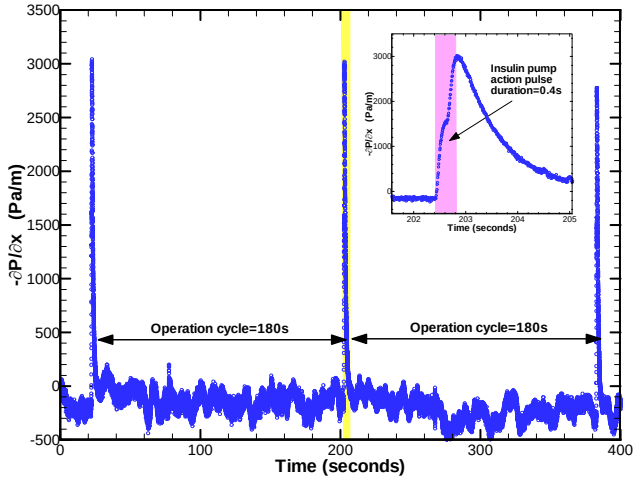

Fig. 8: The measured transient pressure gradient inside the CSII tubing system

Based on the theoretical equations given in Equation (9), an analytical solution of the flow velocity at the centerline of the rectangular microchannel, where *y=W/2* and *z=H/2*, can be written as:

$$U(y,z,t) = \frac{16}{\rho\pi^2}\sum_{n=0}^{\infty}\sum_{m=0}^{\infty}\frac{\sin\frac{(2m+1)\pi}{2}\sin\frac{(2n+1)\pi}{2}}{(2m+1)(2n+1)}\int_0^t f(\tau)e^{-\nu\lambda^2_{mn}(t-\tau)}d\tau \tag{10}$$

Based on the pressure measurement shown in Fig. 8, the transient centerline velocity can be determined numerically from the Equation (10). Fig. 9 shows the analytical solution of the dynamic response of the flow velocity at the centerline of the microchannel along with the micro-PIV measurement results. For the determination of the theoretical solution, the input parameters are carefully selected to be consistent with the

experimental settings. Specifically, the geometry was set as a square duct with $W=H=300\mu m$; the density $\rho=998.2$ kg/m^3 and kinetic viscosity $\nu=1.004\times10^{-6}$ m^2/. The infinite series solution was truncated at m=10 and n=10. It was confirmed that the truncation error is negligible as m≥10 and n≥10.

As shown in Fig 9, both the theoretical solution and the micro-PIV measurement result revealed the similar features in terms of the dynamic response of the centerline flow velocity upon pulsed operation of the insulin pump. The centerline flow velocity was found to increase rapidly as the pump operation pulse starts and reach its peak value at the end of the pump operation pulse. Since no additional pressure head would be built up inside the CSII tubing system after the pump operation pulse, the centerline flow velocity was found to decrease rapidly. It should also be noted that, compared with the micro-PIV measurement results, the theoretical solution predict a much slower decay process for the centerline flow velocity after the pulsed operation of the insulin pump. Further investigation is planned to clarify the discrepancies.

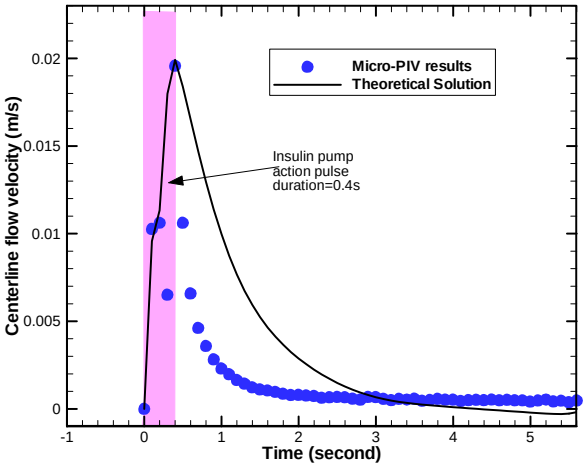

Fig.9: Theoretical prediction of the centerline flow velocity vs. micro-PIV measurement results.

C. EFFECTS OF THE AIR BUBBLES ENTRAINED INSIDE THE CSII TUBING SYSTEM

As aforementioned, it has been suggested that air bubbles entrained into the micro-sized capillary tubing system may reduce or inhibit insulin delivery in CSII therapy. In the present study, an experimental study was also conducted to assess the effects of air bubbles entrained inside the micro-sized CSII tubing system on the insulin delivery. During the experiments, air bubbles were introduced into the CSII tubing system through the reservoir of the insulin pump. The behavior of the air bubbles inside the CSII tubing system upon the pulsed excitation of the insulin pump was monitored. The characteristic changes of the liquid micro-flow due to the air bubbles entrained inside the CSII tubing system were quantified based on the detailed flow field measurements using the micro-PIV technique.

By tracking the movement of the air bubbles inside the CSII tubing system, it was found that the air bubbles were pushed downstream along with the liquid fluid upon the pulsed action of the insulin pump. Eventually, the air bubbles were found to be expelled through the catheter of the infusion set along with the liquid fluid. As described above, the insulin pump was supposed to deliver the same amount (i.e. 1.0μL) of the liquid fluid through the catheter during each action cycle. However, when air bubbles were entrained inside the CSII tubing system, the air bubbles were delivered by the insulin pump, and expelled from the catheter along with the liquid fluid. As a result, the total amount of the liquid fluid actually delivered by the insulin pump was found to be much less than the pre-programmed value due to the existence of the air bubbles. It confirmed that the air bubbles entrained into the CSII tubing system would reduce or even inhibit insulin delivery in CSII therapy.

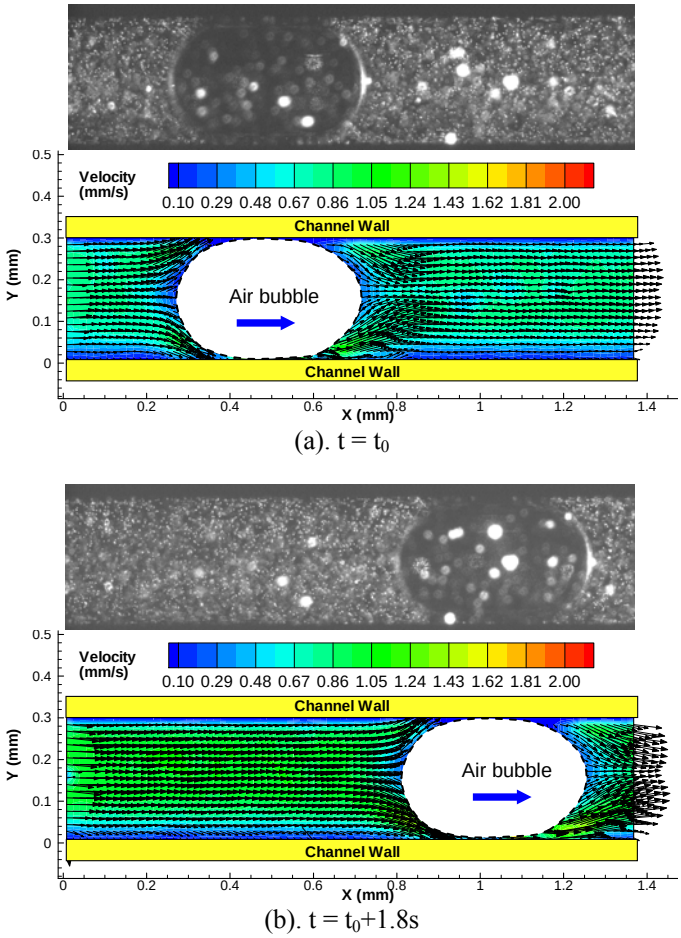

Fig. 10: Micro-PIV measurements around a small migrating air bubble inside the microchannel.

The micro-PIV measurements revealed more interesting features and underlying physics about the effects of air bubbles entrained into the CSII tubing system on the insulin delivery process. Fig. 10 shows two typical micro-PIV measurement results of the flow velocity fields surrounding a small air

bubble entrained inside the microchannel. As shown in the figure, the tip-to-tip length of the air bubble was about 450μm (i.e., ~0.05μL in volume). Cubaud et al. (2006) suggested that an air bubble traveling in a micro-channel may lose their symmetry with respect to the center axis of the channel. As velocity increases, the advancing contact angle increases and the receding contact angle decreases. While the changes of the advancing and receding contact angles at the front and rear ends of the air bubble were not able to be distinguished easily from the acquired micro-PIV images shown in Fig. 10 due to the relatively low flow velocity of the present study, the measured flow velocity vectors around the air bubble reveal the significant changes of the flow features at the rear and front edges of the air bubble clearly. The liquid flow was found to be decelerated and diverge from the centerline along the interface at the rear end of the air bubble, while the liquid flow would be accelerated and converge towards the centerline at the front end. By using the air bubble as the frame of reference, the advancing tip of the air bubble would be a converging stagnation point, whereas the receding tip would be a diverging stagnation point, which agrees with the finding of Yamaguchi et al. (2009) in the study of the ensemble flow fields surrounding a migrating air bubble inside a microchannel.

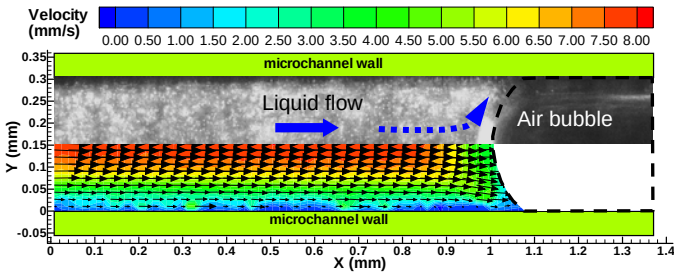

(a). near the rear end of the air bubble

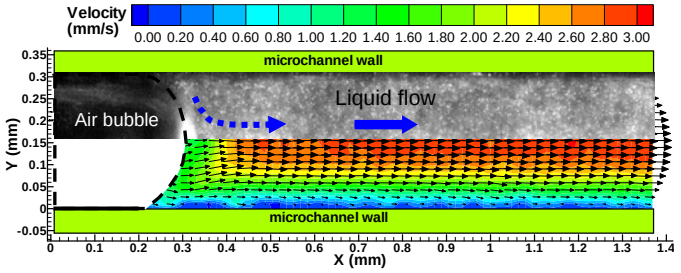

(b). near the front end of the air bubble

Fig. 11: Micro-PIV measurements near the rear and front ends of a long migrating air bubble.

Fig. 11 shows the micro-PIV measurement results near the front and rear ends of a relatively long air bubble entrained inside the CSII tubing system. The tip-to-tip length of the air bubble was found to be about 2.0mm (i.e., ~0.2μL in volume). Again, similar flow patterns can be observed around the long air bubble: the liquid flow would be decelerated and diverge from the centerline along the interface at the rear end of the air bubble, and be accelerated and converge towards the centerline in the region near the front end of the air bubble. This suggests that the flow pattern changes due to the existence of the air bubbles inside the microchannel are mainly influenced by the interfaces between the liquid flow and the air bubbles, which are almost independent of the size of the air bubbles.

Based on the micro-PIV measurement results as those shown in Fig. 11, the normalized flow velocity profiles across the microchannel near the front and rear ends of the migrating air bubble were extracted, which were given in Fig. 12. It can be seen clearly that, the flow velocity profiles in the regions near both rear and front ends of the air bubble were found to change significantly due to the existence of the air bubble. Outside the influential region (i.e. about 0.2mm away from the front and rear ends of the air bubble), the transverse flow velocity profiles were found to stay the same as those shown in Fig. 5 for the case without the air bubble, which can be represented reasonably well by the theoretical solution for a fully-developed laminar channel flow expressed by Equation (1). However, as the liquid flow approaching the rear end of the air bubble, the flow velocity was found to be decelerated and diverge from the channel centerline. As a result, the transverse velocity profiles were found to become much flat. Further towards the interface at the rear end of the air bubble, the flow velocity profiles were found to have apparent deficits in the middle region and two peaks at two sides near the corner regions. As described above, the liquid flow would be accelerated and converge towards the channel centerline in the region near the front end of the air bubble. The acceleration of the liquid flow near the front end of the air bubble can be seen very clearly and quantitatively from the transverse velocity profiles shown in Fig. 9(b). Such measurement results were found to agree with those reported by Miessner et al. (2008) and Yamaguchi et al. (2009) in the studies of two-phase flows in microchannels.

In addition to causing flow pattern changes in the regions near interfaces, the air bubbles inside the CSII tubing system were also found to significantly change the characteristics of the flow decay process after each pulsed action of the insulin pump. As shown clearly in Fig. 13(a), the centerline flow velocity inside the microchannel would decay much more smoothly when no air bubbles were entrained in the CSII tubing system. For the case with air bubbles entrained inside the CSII tubing system, the decay curve was found to become much "noisier" with several "secondary humps" riding on the decay curve. This may be explained by the fact of that the air bubbles entrained inside the CSII tubing system would act as shock-absorbers to change the dynamic response of the micro-flow upon the pulsed action of the insulin pump. While the liquid flow is incompressible, the air bubbles are easily compressed and deformed when the wave front of the tremendous pressure head generated by the pulsed action of the insulin pump approaching the air bubbles. As the pressure wave front passed, the compressed air bubbles would stretch/expand to adjust the pressure difference across the air bubbles. As a result, the velocity decay process of the liquid flow would be affected by the compression and expansion of the air bubbles inside the CSII tubing system. The expansion of the compressed air bubbles could generate small pressure head to accelerate the liquid flow downstream of the air bubbles, which

would result in the "secondary humps" riding on the decay curve as shown in Fig. 13 (a).

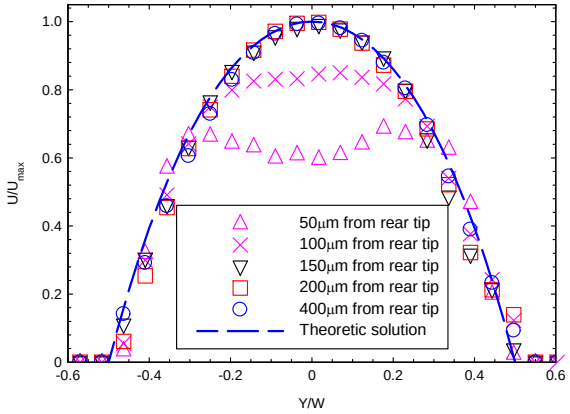

(a). Near the rear end of the air bubble

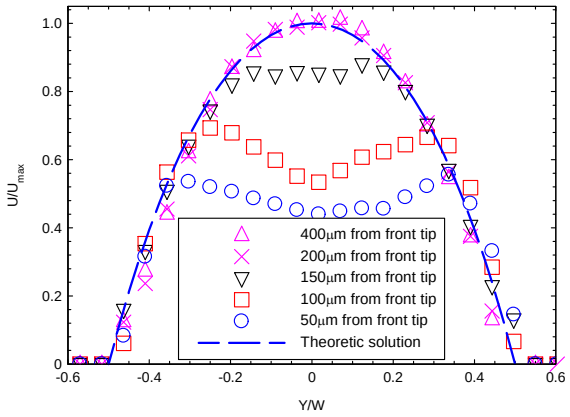

(b). Near the front end of the air bubble

Fig. 12: Measured velocity profiles near the rear and front ends of a long migrating air bubble.

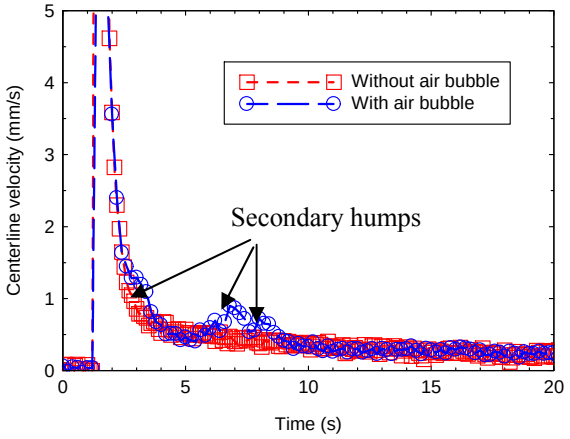

(a). The flow velocity decay curves

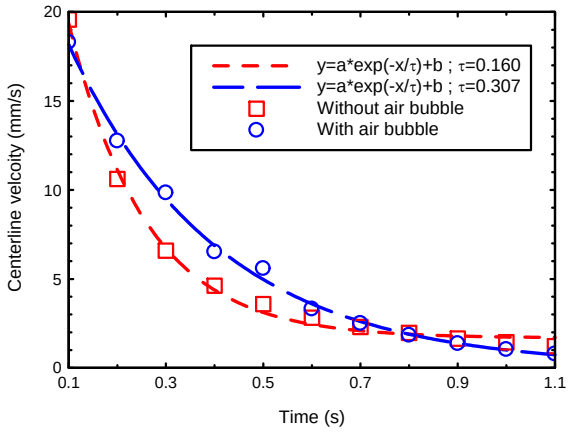

(b). Effects on the initial decay process

Fig. 13: Effects of the air bubble entrainment on the flow decay process

It was also found that the initial flow decay after the pulsed action of the insulin pump would become much slower due to the existence of the air bubbles entrained inside the CSII tubing system. As shown clearly in Fig. 13(b), while the initial flow decay for the case with air bubble entrained inside the CSII tubing system can still be fitted reasonably well by using an exponential function, the characteristic decay time, τ, was found to increase greatly from $\tau = 0.16$s for the case without air bubbles to $\tau = 0.31$s for the case with a ~5.0 mm long air bubble (i.e., 5.0μL in volume) entrained inside the CSII tubing system. The significant change (i.e., almost doubled the value) of the characteristic decay time is believed to be closely related to the change of the compressibility of the microflow due to the existence of the air bubbles inside the CSII tubing system. Compared with the case without air bubbles, the propagation speed of the pulsed pressure waves generated by the pulsed actions of the insulin pump would slow down greatly due to the compressible air bubbles inside the CSII tubing system. As a result, the initial flow decay after the pulsed action of the insulin pump would be retarded due to the existence of the air bubbles inside the CSII tubing system.

CONCLUDING REMARKS

An experimental and theoretical study was conducted to investigate the unsteady microflow driven by an insulin pump commonly used in continuous subcutaneous insulin infusion (CSII) therapy. A micro-PIV system was used to conduct detailed flow velocity field measurements inside a 300μm×300μm microchannel to characterize the transient behavior of the unsteady microflows upon the pulsed actuation of the insulin pump. It was found that the microflow driven by the insulin pump was highly unsteady, which is much more interesting than the creeping flow that the nominal averaged flow velocity would suggest. While the period of the operation cycle of the insulin pump was 180s at the basal rate of 2.0U/H, the real action time of the insulin pump was found to be only about 0.35s. Tremendous pressure head would be generated within the 0.35s operation pulse to push the fluid flow from the reservoir of the insulin pump to the CSII tubing system for insulin delivery. As a result, the flow velocity inside the

infusion tubing system was found to vary significantly during the operation cycle of the insulin pump. As the insulin pump started to operate, the flow velocity within the CSII tubing system was found to increase rapidly. The centerline flow velocity was found to reach 26.4mm/s at the end of the insulin pump action pulse, which is about 260 times higher than the time-averaged flow velocity during each insulin pump operation cycle. The flow velocity within the CSII tubing system was found to decrease swiftly after each pulsed action of the insulin pump. The decay process of the flow velocity was found to be represented well by an exponential function with the characteristic decay time of 0.16s, which is on the same order as the duration time of the operation pulse of the insulin pump. Interestingly, although the magnitude of the flow velocity inside the infusion tubing system was found to decrease rapidly during the flow decay process, the velocity distributions of the micro-flow at different time instants were found to be self-similar. The normalized flow velocity profiles across the microchannel were found to be fit reasonably well by the theoretical solution of a fully-developed laminar channel flow even though the microflow was in transient state during the decay process.

An experimental study was also conducted to assess the effects of the air bubbles entrained inside the CSII tubing system on the insulin delivery. The micro-PIV measurements revealed clearly that the flow patterns of the microflow inside the CSII tubing system would be changed dramatically in the regions near the interfaces between the liquid fluid and the air bubbles. The liquid flow was found to be decelerated and diverge along the interfaces at the rear ends of the migrating air bubbles, whereas the liquid flow at the front ends of the air bubbles would be accelerated and converge towards the channel centerline. It was also found that the total amount of the liquid fluid delivered by the insulin pump through the catheter of the infusion set would become much less than the pre-programmed value due to the existence of the air bubbles inside the CSII tubing system. In addition to reducing the total amount of the liquid fluid delivered by the insulin pump, the air bubbles were also found to act as shock-absorbers to change the dynamic response of the micro-flow upon the pulsed action of the insulin pump. Besides the fact that the flow velocity decay curve would become much "noisier" with several "secondary humps" riding on the decay curve, the initial flow decay after the pulsed action of the insulin pump was found to be retarded greatly (i.e., the characteristic decay time become much longer) due to the existence of the air bubbles inside the CSII tubing system.

ACKNOWLEDGMENTS

The authors also want to thank Dr. Zheyan Jin of Iowa State University for his help in setting up the micro-PIV experiments. The support of National Science Foundation CAREER program under award number of CTS-0545918 is gratefully acknowledged

REFERENCES

Alemzadeh R, Ellis JN, Holzum MK, Parton EA, Wyatt DT (2004) Beneficial Effects of Continuous Subcutaneous Insulin Infusion and Flexible Multiple Daily Insulin Regimen Using Insulin Glargine in Type 1 Diabetes. *Pediatrics* 114(1) 91-95.

Bruttomesso D, Costa S, Baritussio A (2009) Continuous subcutaneous insulin infusion (CSII) 30 years later: still the best option for insulin therapy. *Diabetes Metab Res Rev* 25: 99–111.

Celnik, M.S., Patel, M.J., Pore, M., Scott, D.M., Wilson, D.I., (2006) Modeling laminar pulsed flow for the enhancement of cleaning. Chemical Engineering Science 61, 2079–2084.

Cubaud T, Ulmanella U, Ho CM, (2006) Two-phase flow in microchannels with surface modifications. Fluid Dynamics Research 38, 772–786.

Demuren A, Doane S, (2007) A study of Insulin Occlusion Using the Medtronic MiniMed Paradigm 511 Insulin Pump. *ODU Research Foundation Project Report.*

Demuren A, Gyuricsko E, Diawara N, Castro N, Carter J, Bhaskara R, (2009) Impaired Insulin Delivery During Continuous Subcutaneous Insulin Infusion. *Report to ODU Research Office 2009 Seed Grant.*

Fan C., Chao, BT.(1965). Unsteady, laminar, incompressible flow through rectangular ducts. Zeitschrift für Angewandte Mathematik und Physik 16, 351–369

Gallardo BS, Gupta VK, Eagerton FD, Jong LI, Craig VS (1999) Electrochemical principles for active control of liquids on submillimeter scales. *Science* 283:57–60.

Hartman I (2008) Insulin Analogs: Impact on Treatment Success, Satisfaction, Quality of Life, and Adherence, Clinical Medicine & Research, 6(2) 54-67 doi:10.3121/cmr.2008.793.

Johnson RD, Badr IHA, Barrett G, Lai S, Lu Y, (2001) Development of a fully integrated analysis system for ions based on ion-selective optodes and centrifugal microfluidics. *Anal. Chem.* 73:3940–46.

Kim MJ, Beskok A, Kihm KD (2002) Electro-osmosis-driven micro-channel flows: A comparative study of microscopic particle image velocimetry measuremens and numerical simulations. *Experiments in Fluids* 33:170-180.

Kinoshita H, Kaneda S, Fujii T, Oshima M (2007) Three-dimensional measurement and visualization of internal flow of a moving droplet using confocal micro-PIV. *Lab on a Chip*, 7, 338–346

Li H, Olsen GM, (2006) MicroPIV measurements of turbulent flow in square microchannels with hydraulic diameters from 200 μm to 640 μm, *Int. J. Heat Fluid Flow,* 27, 123–134.

Meinhart CD, Wereley ST, Santiago JG, (1999) PIV measurements of a microchannel flow, Experiments in Fluids 27: 414-419.

Miessner U, Lindken R, Westerweel J, (2008) 3D-Velocity measurements in microscopic two-phase flows by means of

micro-PIV, 14th Int Symp on Applications of Laser Techniques to Fluid Mechanics.

Olsen MG, Bourdon CJ (2003) Out-of-Plane Motion Effects in Microscopic Particle Image Velocimetry. ASME *Journal of Fluids Engineering*. 125: 895-901.

Prins MWJ, Welters WJJ Weekamp JW (2001) Fluid control in multichannel structures by electrocapillary pressure. *Science* 291:277–80.

Poulsen C, Langkjaer L, Worsoe C (2005) Precipitation of Insulin Products Used for Continuous Subcutaneous Insulin Infusion. Diabetes Techno Therapy, 7(1): 142-150 (2005).

Ray, S., Durst, F., (2004). Semianalytical solutions of laminar fully developed pulsating flows through ducts of arbitrary cross sections. Physics of Fluids 16, 4371–4385

Rossetti P, Porcellati F, Fanelli CG, Perriello G, Torlone E, Bolli GB (2008) Superiority of Insulin Analogues versus Human Insulin in the Treatment of Diabetes Mellitus". *Arch Physiol Biochem.* 114(1), 3-14.

Qi, X.G., Scott, D.M., Wilson, D.I., (2008) Modelling laminar pulsed flowin rectangular microchannels, Chemical Engineering Science 63: 2682-2689

Santiago JG, Wereley ST, Meinhart CD, Beebe DJ, Adrian RJ (1998) A micro particle image velocimetry system. Exp Fluids 25: 316-319.

Shalitin S, Phillip M (2008) The Use of Insulin Pump Therapy in the Pediatric Age Group". *Horm Res*. 70, 14-21.

Weissberg-Benchell J, Goodman SS, Lomaglio JA, Zebracki K (2007) The Use of Continuous Subcutaneous Insulin Infusion (CSII): Parental and Professional Perceptions of Self-care Mastery and Autonomy in Children and Adolescents. *Journal of Pediatric Psychology* 32(10) 1196–1202.

White F (1991) Viscous Fluid Flow, Mcgraw-Hill, 2nd Edition.

Wolpert HA, Faradji RN, Bonner WS, Lipes MA (2002) Metabolic decompensation in pump users due to lispro insulin precipitation. BMJ 324:1253.

Yamaguchi E, Smith BJ, Gaver DP (2009) μ-PIV measurements of the ensemble flow fields surrounding a migrating semi-infinite bubble, Exp Fluids 47:309-320.